Mantle kinematics driving collisional subduction: Insights from analogue modeling

Paul Pitard [a], Anne Replumaz [a,*], Francesca Funiciello [b], Laurent Husson [a], Claudio Faccenna [b]

[a] ISTerre (Institut des Sciences de la Terre), Université Grenoble Alpes, CNRS, F-38000 Grenoble, France
[b] Dipartimento Scienze, Università degli Studi Roma TRE, Largo S. Leonardo Murialdo 1, 00146 Rome, Italy

A R T I C L E   I N F O

A B S T R A C T

Since several decades, the processes allowing for the subduction of the continental lithosphere less dense than the mantle in a collision context have been widely explored, but models that are based upon the premise that slab pull is the prominent driver of plate tectonics fail. The India–Asia collision, where several episodes of continental subduction have been documented, constitute a case study for alternative views. One of these episodes occurred in the early collision time within the Asian plate where continental lithosphere not attached to any oceanic lithosphere subducted southward in front of the Indian lithosphere during its northward subduction that followed the oceanic subduction of the Tethys ocean. This process, known as collisional subduction, has a counter-intuitive behavior since the subduction is not driven by slab pull. It has been speculated that the mantle circulation can play an important role in triggering collisional subduction but a detailed, qualitative analysis of it is not available, yet. In this work we explore the southward subduction dynamics of the Asian lithosphere below Tibet by means of analogue experiments with the aim to highlight how the mantle circulation induces or responds to collisional subduction. We found that during the northward oceanic subduction (analogue of Tethys subduction) attached to the indenter (Indian analogue), the main component of slab motion is driven vertically by its negative buoyancy, while the trench rolls back. In the mantle the convective pattern consists in a pair of wide convective cells on both sides of the slab. But when the indenter starts to bend and plunge in the mantle, trench motion reverses. Its advance transmits the far field forces to two upper plates (Asian analogues). The more viscous frontal plate thickens, and the less viscous hinterland plate, which is attached to the back wall of the box, subducts. During this transition, a pair of sub-lithospheric convective cells is observed on both sides of the Asian analogue slab, driven by the shortening of the frontal plate. It favors the initiation of the backwall plate subduction. Such subduction is maintained during the entire collision by a wide cell with a mostly horizontal mantle flow below Tibet, passively advecting the Asian analogue slab. Experimental results suggest that once the tectonic far-field force related to the forward horizontal motion becomes dominant upon the buoyancy forces, trench advancing and the transmission of the tectonic force to the upper and backwall plates are promoted. This peculiar condition triggers the subduction of the backwall plate, despite it is light and buoyant.

© 2018 Elsevier B.V. All rights reserved.

1. Introduction

Continental subduction has been proposed for decades as a key process occurring during the long-lasting collision between India and Asia, with a northward motion of India at a rate in excess of 50 mm/yr since ∼50 Ma (e.g. Patriat and Achache, 1984; Molnar and Stock, 2009; van Hinsbergen et al., 2005), allowing the

subduction of the continental lower crust attached to the lithospheric mantle while the upper crust thickens and forms the Tibetan plateau (e.g. Mattauer, 1986; Tapponnier et al., 2001). However, only recently some evidence of such process has been collected. The fact that the continental lithosphere could subduct has first been hypothesized from the seismicity within the continental collision framework of the Pamir and Hindu Kush at the western extremity of the collision system, which reveals two subduction zones of opposite vergence (Chatelain et al., 1980; Burtman and Molnar, 1993). However, the nature of the lithosphere, continental or oceanic, remained speculative, as well as

* Corresponding author.
  E-mail address: anne.replumaz@univ-grenoble-alpes.fr (A. Replumaz).

the slab length. Global P-waves tomography allows to discuss the maximum depth extent of the two distinct slabs (Negredo et al., 2007): the Indian slab deepens northward almost vertically down to ~600 km beneath the Hindu Kush, and the Asian lithosphere is seemingly deepening southward down to ~400 km beneath the Pamir (Fig. 1). The maximum depth of seismicity has been modeled and shown to be compatible with continental lithosphere subduction (Negredo et al., 2007). Recent seismic studies of the Pamir–Hindu Kush region show details of the lithospheric structure of such slabs (Mechie et al., 2012; Kufner et al., 2016), revealing a strong evidence of their continental nature by showing the subduction of light continental lower crust on top of denser continental upper lithosphere down to ~400 km depth (Schneider et al., 2013). Although less documented, the Asian lithosphere in central Tibet is inferred to subduct southward down to 300 km, with no related seismicity (Kind et al., 2002; Replumaz et al., 2013). During the early Tibetan collision stage, a first episode of subduction of the Asian lithosphere likely occurred beneath Qiangtang, as recorded by Cenozoic volcanics between 50 and 30 Ma in the Qiangtang block (e.g. DeCelles et al., 2002; Spurlin et al., 2005; Goussin et al., submitted for publication) (Fig. 1). This slab detached, and sunk, and is possibly revealed by a positive P-wave speed anomaly in the lower mantle (Replumaz et al., 2013) (Fig. 1).

Beneath the Himalaya, it has been proposed that at present-day the Indian lower crust, attached to its lithospheric mantle, is bent and is underplated below southern Tibet (Nábělek et al., 2009) (Fig. 1). A possible additional process that may help the subduction of continental plates it eclogitization. During the bending of the Indian plate beneath the Himalaya, its density could be close to mantle density, which favors underplating below southern Tibet (Hetenyi et al., 2007).

However, a dynamic explanation of continental subduction is still lacking, mostly because it is in principle less dense than the mantle (in the absence of secondary processes like eclogitization). Deciphering its contribution to the formation of the Tibetan plateau where this under-explored process is possibly important (Mattauer, 1986; Tapponnier et al., 2001; Spurlin et al., 2005; Replumaz et al., 2013; Goussin et al., submitted for publication). But above all, this observation calls for to go beyond the paradigm of slab pull as a unique driver of plate tectonics. Alvarez (2010) already pointed to the fact that protracted collisions require support from mantle tractions; sustained continental subduction is even more difficult to sustain under the premise that slab pull is the prominent, if not unique, tectonic engine.

A low-density contrast between the continental lithosphere and the mantle facilitates the subduction of the continental lithosphere attached to a dense oceanic slab (Capitanio et al., 2010; Bajolet et al., 2013), but it cannot trigger the subduction of the Asian lithosphere which is not attached to a dense slab (Fig. 1). At the lithospheric scale, analogue models show that the initiation of continental subduction in a context of convergence occurs with a low degree of coupling at the plate interface and with an inclined plate contact (while vertical boundary favor buckling of the lithospheres) (Luth et al., 2010; Willingshofer et al., 2013). At the mantle scale to date, only two models attempt to quantita-
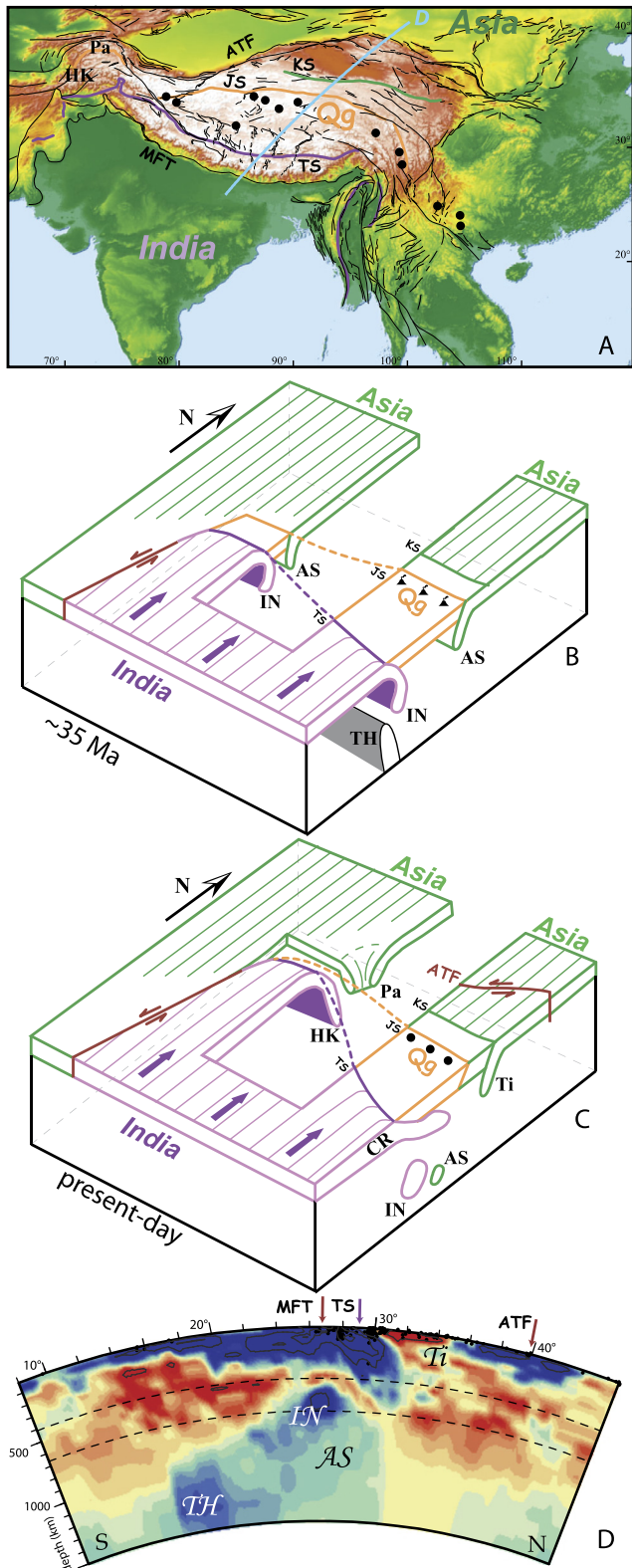
Fig. 1. (A) Topographic map of the collision zone between India and Asia. The Indian crust is separated from the Asian crust by the Tsangpo suture (TS, in purple). In central Tibet, Cenozoic volcanic rocks between 50 and 30 Ma (black dots) are observed north of the Qiangtang block (Qg), located south of the Jinsha suture (JS, in orange). KS: Kunlun suture, Pa: Pamir, HK: Hindu Kush. (B) Three-dimensional schematic view of the lithospheric structure (middle-lower crust and lithospheric mantle) below Tibet in the early collision time. The Indian lithosphere (IN) subducted northward facing the Asian slab (AS) beneath Qiangtang (Qg). Both slabs detached from the continents and have sunk down to the lower mantle since then. The same color code used for the different plates is applied to experimental data. (C) Three-dimensional schematic view of the lithospheric structure at present-day as inferred from global tomographic cross section (Replumaz et al., 2013) shown below, showing to the southwest, the Indian lithosphere (in purple) subducting northward beneath the Hindu Kush (HK) down to the transition zone (~600 km), facing the Asian lithosphere (in green) subducting beneath Pamir down to 300–400 km. In central Tibet, the Asian lithosphere (Ti, in green) is subducting southward down to 300 km along the Kunlun suture (KS), facing the Indian craton (CR) underplating south Tibet. (D) Cross-section along line shown on A of Pwave global tomographic model, with positive anomalies interpreted as slabs subducted during the collision (Replumaz et al., 2013). (For interpretation of the colors in the figure(s), the reader is referred to the web version of this article.)

Fig. 2. Experimental setup, three-dimensional view of the initial stage (C), and top (A) and side (B) views during experiment.

tively explain this process on a long-term collision time scale. First, a three-dimensional analogue model analyses the subduction dynamics of a light li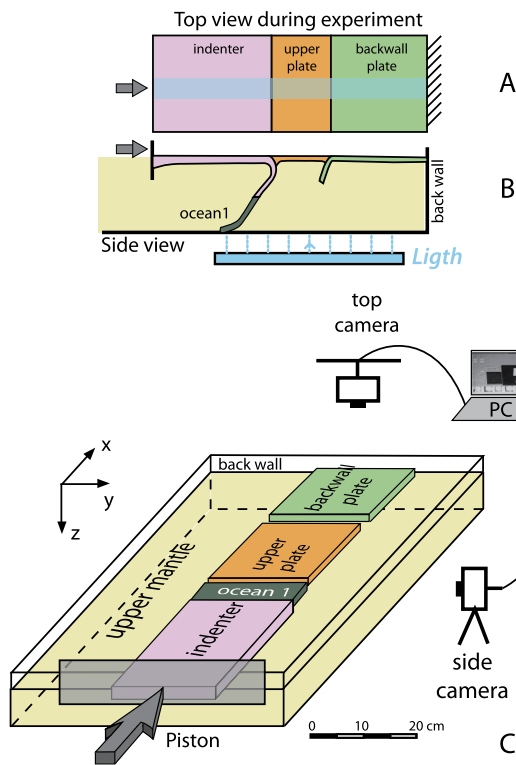thosphere, analogue of the Asian plate, below Qiangtang. This model explores the geodynamic contexts wherein such atypical subduction may occur (different density of plates, attached or not to an oceanic plate) without exploring the underlying mantle dynamics (Replumaz et al., 2016). The second is a 3D numerical model of the Hindu Kush–Pamir orogenic system specifically exploring the role of the complex geometry of the regional subduction zone, slab-curvatures in particular (Liao et al., 2017). Here, we present experimental results on the Asian lithosphere subduction, focusing on the subduction induced mantle circulation active in this geodynamic environment, obtained using the same geometry setup than Replumaz et al. (2016) but with passive markers in the mantle analogue showing this circulation. We opt for this very simple initial geometry, featuring two linear subduction zones of opposite vergences (Fig. 2), similar to the supposed geometry of in Central Tibet in the early collision time (Fig. 1). Our models highlight the deep mantle contribution to the collisional subduction in a simple context of frontal collision, equivalent to

the collision between India and Asia. They provide an explanation for the subduction of a light and buoyant continental lithosphere into the mantle in a collision context, emphasizing the role of far field forces instead of subduction related forces, typically slab pull. Most importantly, this process obviously rules out slab pull as the omnipotent driver of plate tectonics and calls back to the more ancient *conveyor belt* view advocated by Holmes (1929).

2. Model setup and experimental procedure

The model is composed of thin sheets of silicone putty as analogs for the lithospheres, lying on top of low-viscosity glucose syrup that simulates the rheology of the asthenospheric mantle. Silicone putties are visco-elastic materials, quasi-Newtonian at experimental strain rates (Weijermars, 1986) and the glucose syrup a Newtonian fluid. The properties of analog materials are listed in Table 1. The viscosity and density of silicone and syrup are constant and are considered as average effective values.

The experimental setup consists of a Plexiglas tank filled with 11 cm of glucose syrup, corresponding to the upper mantle in nature (i.e., 660 km), on top of which three silicone plates rest, and represent the lithosphere (Fig. 2). The indenter plate is made of two adjacent silicones: a silicone unit which is denser than the underlying syrup, that is analogue to the Tethys oceanic lithosphere (referred to as *ocean* in the following), and an adjacent silicone unit which is conversely less dense than the syrup and is analogue to the Indian continental lithosphere (referred to as *indenter*). The trailing edge of the low-density silicone is attached to a piston which is advancing forward at constant velocity. At the back of the box, the *backwall* plate is made of a light silicone which is analogue of northern Tibet, the trailing edge of which is fixed to the back wall of the tank. A third silicone plate, less dense and less viscous than the backwall plate, analogue to the southern Tibet lithosphere, is disposed between the indenting plate and the backwall plate, and is referred to as *upper plate*. The indenter, the upper and the backwall plate are not welded at the onset of the model and their edges are lubricated with Vaseline to minimize any possible plate-plate sticking. In the initial configuration, the leading edge of the silicone plate is forced downwards inside the syrup with opposite vergence for the oceanic plate and the backwall plate (Fig. 2A), as a means to start the subduction process, making the initiation of subduction beyond the scope of this paper. Nevertheless our setup adequately reproduces the shape of the lithosphere along a suture, making a discontinuity at the scale of the lithosphere.

The experiments are scaled for gravity, length, density, viscosity and velocity following previous studies (e.g. Weijermars and Schmeling, 1986; Funiciello et al., 2003). The scaling factor for length is 1.7×10^{-7} so that 1 mm of the model corresponds to 6 km in nature (for example, the upper mantle thickness is 110 mm in model and 660 km in nature). The density and vis-

Table 1
Materials properties and experiments scaling (see also Bajolet et al., 2013; Replumaz et al., 2016).

	Indenter	Ocean	Upper plate	Back wall plate	Mantle
Exp. 1	$20 \cdot 25 \cdot 1.1$ cm³	$20 \cdot 7 \cdot 1.1$ cm³	$20 \cdot 10 \cdot 0.8$ cm³	$20 \cdot 20 \cdot 0.8$ cm³	$45 \cdot 55 \cdot 11$ cm³
	$\rho = 1402$ kg/m³	1508	1397	1402	1428
	$\mu = 2 \times 10^5$ Pa s	3.3×10^4	2.9×10^4	2×10^5	30

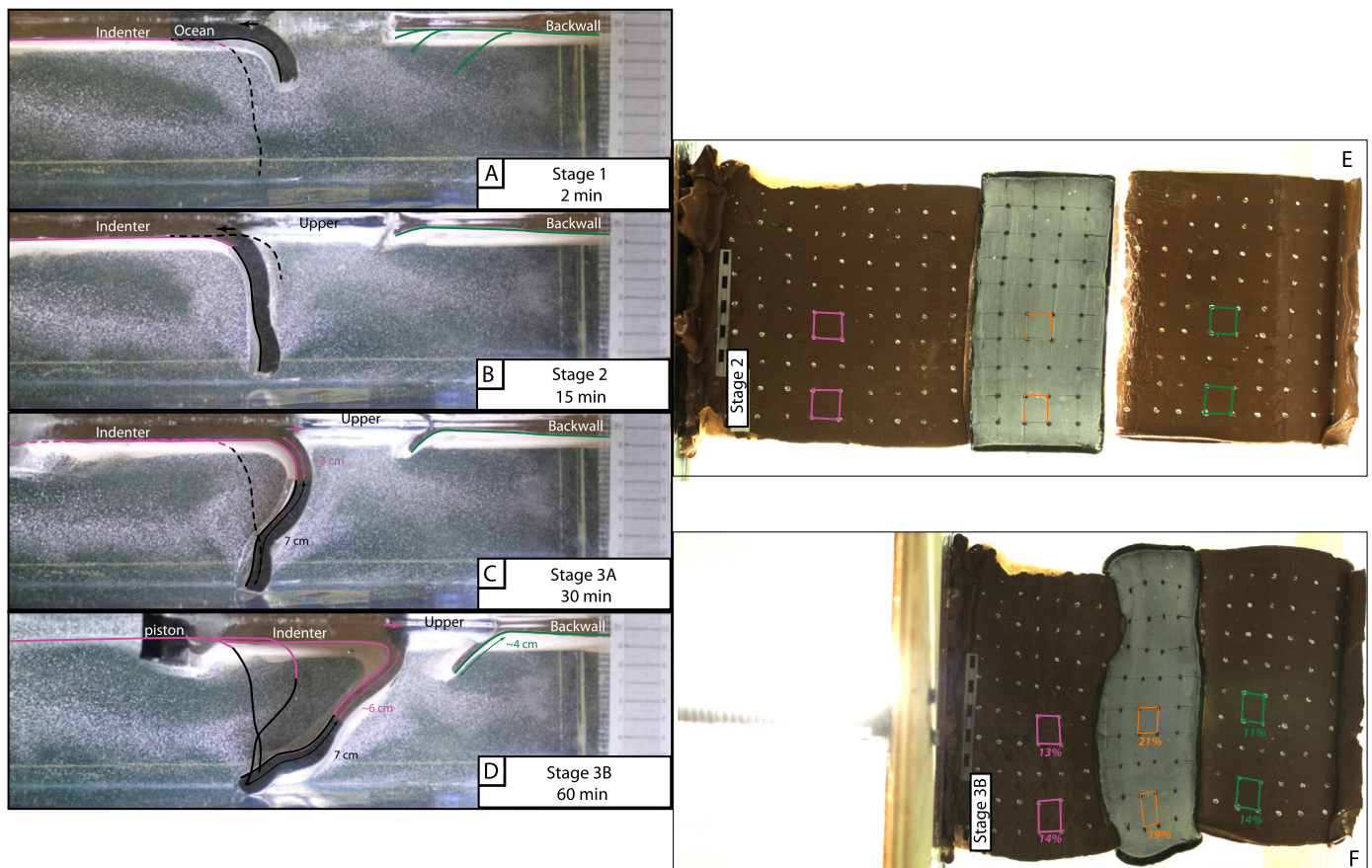|	Dimensionless parameters		Equivalence model-nature
$L°$	Characteristic length: L_{model}/L_{nature}		1.7×10^{-7}
$t°$	Characteristic time: $(t_{model}/t_{nature}) = (\Delta\rho gh)_{lith\ nature}/(\Delta\rho gh)_{lith\ model} \times (\eta_{l\ model}/\eta_{l\ nature})$		1 min$_{model} \to 0.55$ My$_{nature}$
$U°$	Characteristic velocity: $(U_{model}/U_{nature}) = t_{nature}/t_{model} \times L_{model}/L_{nature}$		1 cm h^{-1} $_{model} \to 0.18$ cm y^{-1} $_{nature}$

Fig. 3. (A–D) Side view photos of experiment 1, showing successive position of the ocean (underlined in black), indenter (in pink), upper and back wall (in green) slabs. Trench rolls back of the ocean during the first stage is shown by a black arrow, trench advance of the indenter during the rest of the experiment is shown by a pink arrow. (D) Slab lengths at 60 min shown by arrow along the slabs. Bright dots are air micro-bubbles used as passive tracers, lighted from below. (E) top view photos for stage 2, showing the initial grid of passive markers drawn on the silicone layers approximately 2 cm ∗ 2 cm with 2 squares chosen to estimate the thickening of the plates during the experiment (for the indenter in pink, the upper plate in orange, and the backwall plate in green). (F) top view photo for stage 3B, showing the thickening of the 3 continental plates in percent.

cosity ratios between the oceanic silicone putty and the mantle glucose syrup are 1.05 and 1.5×10^3 respectively (Table 1). The piston advances at a rate of 0.54 cm min^{-1} which corresponds to a convergence rate of 5.7 cm yr^{-1} in nature, mimicking the northward motion of India at a rate in excess of 50 mm/yr (e.g. Patriat and Achache, 1984; Molnar and Stock, 2009; van Hinsbergen et al., 2005); 1 min in experimental time correspond to 0.55 Myr in nature. The selected lithosphere-mantle viscosity contrast represents an upper bound when compared with the natural prototype, which implies that the slab-mantle coupling is minimized while the slab-induced mantle circulation is enhanced (Funiciello et al., 2006).

Each experiment is monitored over its entire duration by top and lateral snapshot views taken at regular time intervals, which enables us to quantify the amount of subducted lithosphere, the thickening of the plates, and the flow field (Fig. 2). The glucose syrup, analogue to the upper mantle, is preliminary seeded with bright reflecting air micro-bubbles that behave as passive tracers when enlightened from the bottom of the box by a narrow laser beam located along the centerline of the system (Fig. 2). These bubbles have a diameter less than 1 mm, so that their possible influence on the density/viscosity is negligible (Funiciello et al., 2006). Post-processing of side views is made using PIVlab, a time-resolved digital particle image velocimetry tool of Matlab, which provides sparse velocity vectors using the bright passive tracers seeding the mantle (Thielicke and Stamhuis, 2014). The velocity field is measured in 2D, along the vertical center plane of the model and shows the poloidal component of the flow. This model was not designed to monitor the toroidal component of

the mantle flowing off the center plane of measurement, as we light the silicone from below it is not possible to resolve the flux from above, which thus has been not recorded. We only make a qualitative interpretation of this component, shown and quantified in some previously published paper (e.g. Funiciello et al., 2004; Piromallo et al., 2005; Husson et al., 2012a).

3. Experimental results: mantle flux related to collisional subduction

In this paper we present in detail the result of one model (Fig. 3) reproducing the reference model of Replumaz et al. (2016), which is the most similar to what is observed in Tibet. This experiment is part of an experimental series of 18 models, 15 without micro-bubbles in the syrup, 3 of them published in Replumaz et al. (2016), the complete list published in supplementary material, 3 models done with micro-bubbles, which has been designed with a particular focus on mantle flow during collisional subduction using passive markers lighten by below (Fig. 2).

The evolution of this model follows 3 stages. During the first stage, the oceanic part of the indenter plate subducts under its own weight into the syrup (Fig. 3A). During that stage, the dip of the slab rapidly increases because the trench rolls back at a lower rate than the forward motion of the piston; this triggers regional scale mantle circulation. The mantle flux shows a classic pair of convective cells on both sides of the oceanic slab extending along the entire box depth (Fig. 4A). The convective cell under the indenter plate (cell 1a) has the highest velocity (mean value ∼3.5
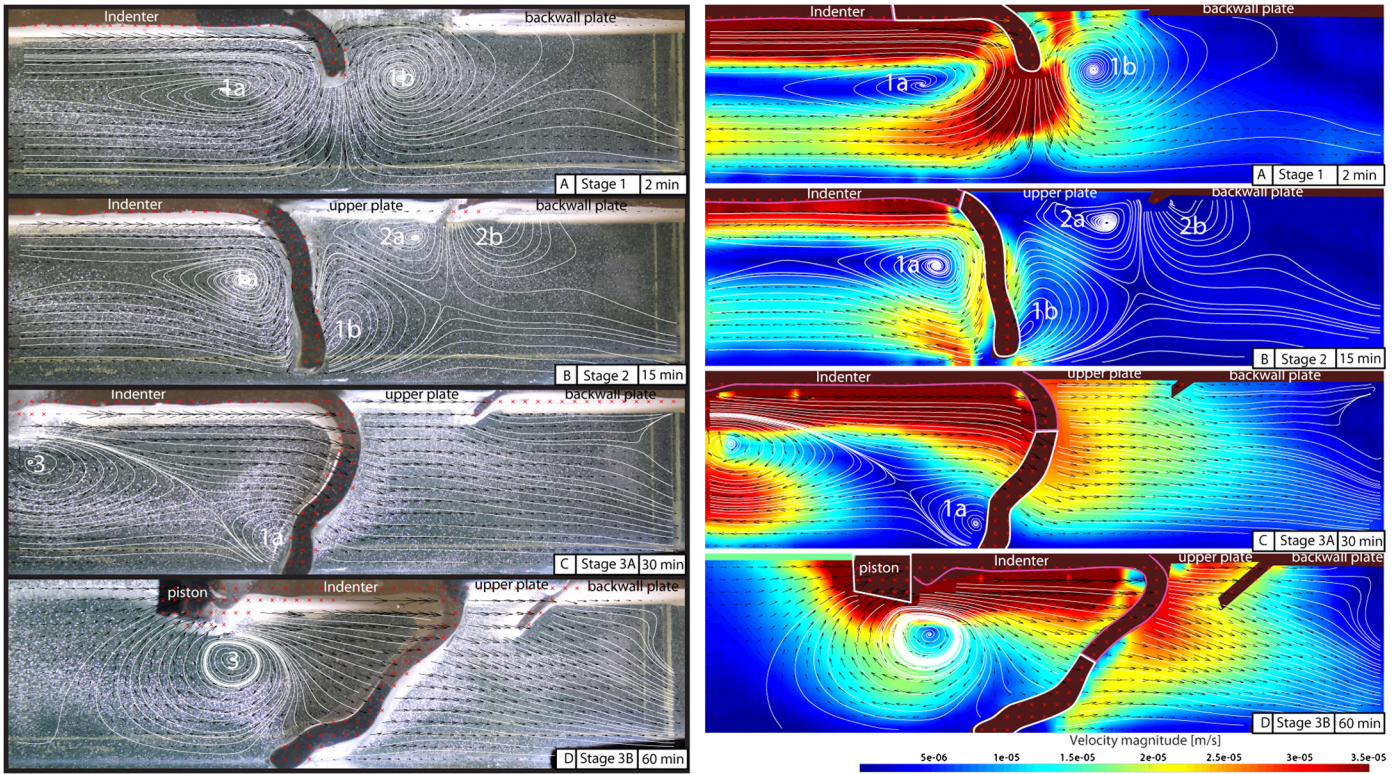
Fig. 4. (A–D) Poloidal (2D in the vertical plane) velocity field of the glucose syrup, showing convective cells (white number). Images of the micro-bubbles are recorded by the lateral camera and post-processed to obtain a time-resolved digital particle image velocimetry of the micro-bubbles, providing sparse velocity vectors of the mantle flow (black arrow), not available for the plates (red cross). (E–H) Velocity field (black arrow), velocity magnitude (color scale), and flow streamlines (white isocontours). Outlines of indenter plate in pink and oceanic plate attached to indenter in white.

10^{-5} m/s, Fig. 4B), sheared from the top by the forward advancing indenter ($u_{indenter} = 5 \ 10^{-5}$ m/s) and further excited on its lateral side by the vertical descent of the oceanic slab ($v_{ocean} = 7 \ 10^{-5}$ m/s). The convective cell below the upper and backwall plates (cell 1b) has a mean velocity magnitude of $\sim$1.5 10^{-5} m/s, more than twice slower, excited along its lateral side by the descent of the dense slab, and to the top by slab roll back (at a slower horizontal velocity, $u_{roll \ back} = 2 \ 10^{-5}$ m/s). During this stage the flow is dominated by the poloidal component, as revealed in our 2D view.

The second stage is a transition phase, occurring 15′ after the beginning of the model. During this stage the oceanic slab reaches the bottom of the box while the continental indenter starts to curve and plunge into the syrup (Fig. 3B). The inception of the positively buoyant indenter in the subduction zone reverses the motion of the trench which starts to advance toward the upper plate at a horizontal velocity of $u_{indenter} = 3.6 \ 10^{-5}$ m/s. Trench advance of the indenter plate forces the backwall plate to subduct. The lower boundary (bottom of the box) represents an intermediate condition between a free slip and no slip boundary condition for the slab, generating only a partial anchoring of the slab at bottom of the box. Such partial anchoring allows both retreating and advancing of the trench motion but is not favoring the switch between both trench motions (e.g. Bellahsen et al., 2005). The reverse motion observed during our experiments, from trench retreat during oceanic subduction to trench advance during continental subduction is triggered by the specificity of our setup: the continental subduction. During this stage the mantle convective pattern reshuffles and becomes more articulated, with 2 pairs of convective cells related to both slabs (Fig. 4B). The pair of convective cells related to the slab belonging to the indenter plate is asymmetric: a wide cell is observed below the indenter similar to the one of the first stage (cell 1a) while a smaller convective cell appears below

the upper plate, in the deeper half of the box where the oceanic slab still shows a vertical component of the subduction velocity (cell 1b). The second pair of convective cells surrounds the backwall slab. These asymmetric cells are located only in the shallowest half of the box. The velocity is one order of magnitude lower than in cell 1a (mean value $\sim$5 × 10^{-6} m/s), and their life span is very short. The convective cell underneath the upper plate (cell 2a) responds to the surface drag caused by the shortening of the upper plate starting at this stage, and is driven by trench advance that forces contraction (Fig. 4B). This shallow convective cell generates a downward flow at the margin between the upper and backwall plates. This downward flow could initiate the downward motion of the backwall plate at the interface between the two plates. The cell which is located below the backwall plate (cell 2b) is less developed, as no shortening of the backwall plate occurs at that stage, and only responds to the descent of the backwall plate in the mantle. During this stage the flow is also dominated by the poloidal component.

The third stage of model evolution presents a continuous trench advance of the continental indenter slab and a continuous subduction of the backwall plate. The subduction of the indenter enhances slab curvature during the rest of the experiment (Fig. 3C&D). The convective pattern changes radically, with no more pair of cells but a dominant horizontal motion of the mantle, which is dragged from above by the indenter (Fig. 4C&D). It is advancing at a mean horizontal velocity of $u_{indenter} = 3.8 \times 10^{-5}$ m/s. The horizontal flow under the upper and backwall plates has a maximum velocity of $\sim$2.5 × 10^{-5} m/s close to the indenter, decreasing gradually toward the back wall (Fig. 4C). The flow underneath the upper and backwall plates is entirely forward in the central section of the box, and is confined in the 2D plane between the advancing indenter slab and back wall of the box. Importantly, this implies that the return flow is entirely toroidal, i.e. sideways from the subducting

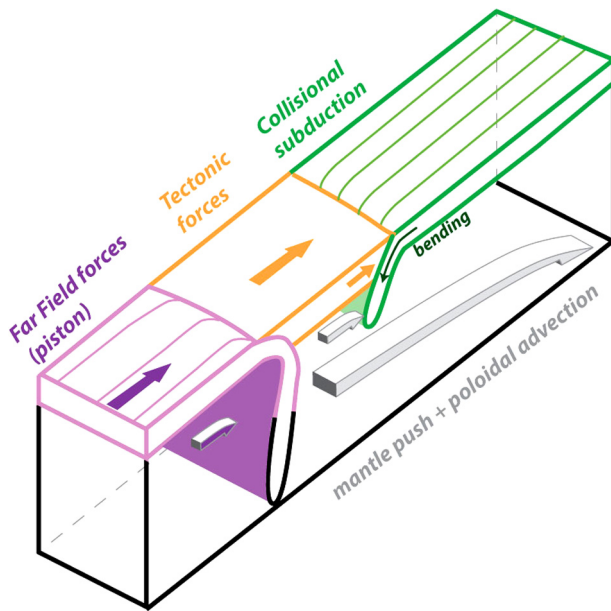**Fig. 5.** Schematic view of mantle flux related to collisional subduction in the middle of the experimental box, analogue of the processes acting in the central part of the continental collisional system inferred to occur beneath Tibet, focusing on the poloidal component of the mantle flux for which the experiment has been designed.

slab. During the transition, as the indenter advances, the toroidal flow overcomes the poloidal flow observed in the previous stages which was driven by the oceanic subduction. A residual poloidal cell 1a is observed at the bottom of the box, with a downward vertical component of velocity along the oceanic slab (mean value $\sim 5 \times 10^{-6}$ m/s). The convective cell observed below the piston is a boundary effect of our experimental setup that we let aside. During this stage, the slab that belongs to the backwall plate is passively transported (advection) by this horizontal mantle flow, not perturbed by the slab. When the length of the slab increases, the flow is slightly perturbed by the slab (Fig. 4D). The flow is faster upstream of the slab than downstream so that a dynamic mantle push occurred on the backwall slab (Fig. 5). The backwall slab velocity of subduction is constant, $u_{back} = 2.3 \times 10^{-5}$ m/s.

Between 15′ and 60′ min, the indenter slab reaches $\sim$5 cm depth in the box, while the backwall slab reaches about half of it ($\sim$2.5 cm depth with a $\sim$4 cm long slab), corresponding to a mean vertical component of velocity of $v_{back} \sim 10^{-5}$ m/s, half that of the indenter. Plate thickening is propagating northward during the experiment, first with the thickening of the indenter plate, followed by thickening of the upper plate, and finally by that of the backwall plate. From the top views, a squared grid of passive markers drawn on the silicone layers enables to quantify the amount of subducted lithosphere and the area variation of each square during the experiment (Fig. 3). For one given square, the thickening is calculated using the initial and final values of area, and the initial thickness of the plate, assuming homogeneous thickening. At the end of the experiment the more viscous upper plate has thickened by 19–21%, the less viscous indenter plate by 13–14%, the backwall plate made of the same silicone by 11–14% (for detailed measurement and analysis of the thickening process, see Replumaz et al., 2016).

4. How is the collisional subduction driven?

Despite evidence for subduction of positively buoyant continental lithosphere, inferring the dynamics of such a counter-intuitive process is not clear yet. Indeed, when such a plate subducts, its

buoyancy is positive and is not a driving force. The slab buoyancy is proportional to the density contrast ($\Delta\rho$) between the silicone plate and the glucose syrup ($\rho = 1428$ kg/m^3), gravity acceleration ($g = 10$ m/s^2), and slab thickness (h) and length (l) (e.g. Turcotte and Schubert, 1982). Considering a plate lighter than the syrup ($\rho = 1402$ kg/m^3), the slab buoyancy is positive, increasing with slab length. For the backwall slab, the maximum value of the slab buoyancy is $\sim$0.08 N/m ($h = 8$ mm, $l = \sim$4 cm maximum). This positive buoyancy cannot drive the subduction of the backwall plate, for it is even a resisting force.

Another engine has to drive the collisional subduction. In our models, this engine is the push of the piston (Fig. 2). The piston drives the indenter plate at a constant velocity. The push of the piston is transmitted to the indenter plate which shows a high horizontal motion during the entire evolution of the experiment (Fig. 4). This push mimics far-field tectonic forces. When the indenter plunges into the mantle, the trench begins to move forward, transmitting the push of the indenter to the upper plate. First the upper plate absorbs this motion by thickening (stage 2), then it transmits the motion to the backwall plate, which is forced to subduct. Because the indenter is forced to move forward at a prescribed rate, the tectonic force adjusts to overcome the resisting forces and sets a force balance that allows for the convergence to occur at the prescribed rate. At the lithospheric scale, the main resisting forces acting on the backwall slab are the bending resistance and the lithosphere/lithosphere interface resistance between the back wall and the upper plates (e.g. Funiciello et al., 2003; Luth et al., 2010; Willingshofer et al., 2013). In our experiment, the push of the upper plate on the backwall plate hinge instantaneously adjusts to overcome these resisting forces, thereby allowing for bending and plunging in the mantle. The efficiency of the downward subduction in the mantle is favored by a low viscosity contrast across the LAB, leading to the initiation of the backwall subduction.

The buoyancy force of the indenter slab is also positive, as for the backwall slab, with a maximum value of $\sim$0.17 N/m ($\rho = 1402$ kg/m^3, $h = 1.1$ cm, $l = \sim$6 cm). But as the indenter slab is attached to the oceanic slab, with a strong negative contrast compared to the mantle (buoyancy force value of -0.6 N/m with $\rho = 1508$ kg/m^3, $h = 1.1$ cm, $l = 7$ cm), the cumulative buoyancy for the indenter/oceanic slab remains negative throughout the entire course of the experiment (-0.43 N/m minimum). The negative buoyancy of the oceanic slab is sufficient to pull it in the mantle (e.g. Turcotte and Schubert, 1982). Evolving in a self-consistent way with a balance between buoyancy and viscous forces of the entire system, this slab pull also generates trench retreat, due to the roll back of the slab under its own weight (Funiciello et al., 2003). In our experiment, trench retreat is impeded by the forward advance of the piston (Fig. 3). When the indenter reaches the trench, the forward horizontal motion becomes dominant, despite a cumulative negative buoyancy for the indenter/oceanic slab. The tectonic force becomes dominant upon the buoyancy force, which promotes trench advance and the transmission of the tectonic force to the upper and backwall plates. They provide an explanation for the subduction of a light and buoyant continental lithosphere into the mantle in a collision context, emphasizing the role of far field forces instead of subduction related forces, slab pull in particular.

5. Comparison with natural system

Mounting evidence for subduction of positively buoyant continental lithosphere is available (e.g. Kind et al., 2002; Hetenyi et al., 2007; Mechie et al., 2012; Kufner et al., 2016; Schneider et al., 2013). At the mantle scale, simple models have been proposed, showing that a low density contrast between the continental lithosphere and the mantle facilitates the subduction of the Indian

continental lithosphere attached to a dense oceanic slab (Capitanio et al., 2010; Bajolet et al., 2013), even after partial or complete breakoff between the Indian plate and the oceanic plate (Capitanio et al., 2015). Yet, it remains insufficient to trigger the subduction of the Asian continental lithosphere, which is not attached to a dense slab (Fig. 1). Recent 3D numerical geodynamic models of the Hindu Kush–Pamir orogenic system show that the Asian lower crust is also able to subduct not attached to a dense slab, but in a very peculiar context with a complex initial subduction-zone geometry corresponding to this region, to explain the curvature of the Pamir slab (Liao et al., 2017). In this paper we focus only on 2D-like analysis of the process along a north–south cross section, avoiding to touch complex 3D aspects that cannot be properly simulated by our simplified models.

Our analogue experiments consist of a simplified initial geometry of two linear subduction zones of opposite vergences (Fig. 2), similar to the supposed setting of the lithospheres in Central Tibet in the early collision time (Fig. 1). They show that the subduction of continental lithosphere lighter than the mantle is dynamically sustainable, provided that an additional contribution forces the system to subduct. In our experiments, far field forces are responsible for sustained trench advance during collision, and subsequently force the subduction of continental units into the mantle (Fig. 5). This forced subduction takes advantages of weaker zones, such as suture zones, which in our experiments, are materialized by a discontinuity between the upper plate and the backwall plate of different density (Fig. 2). This setting resembles the case of the Tibetan plateau, which is made of several blocks separated by different suture zones (Fig. 1). The differential thickening that occurs between 2 plates of different viscosities, generates shallow lithospheric convective cells, which in turns favor the initiation of the subduction of the more viscous back plate (Fig. 4B). Furthermore the thickening of the upper plate could form a backstop to the backwall plate enhancing the initiation of its subduction. In previously published model (experiment 3 in Replumaz et al., 2016) with a setup characterized by a lower upper plate viscosity, a strong thickening of this plate occurred, absorbing a higher portion of the far field forces in that case, but also leading to the subduction of the backwall plate. Such rheological contrast is observed in Tibet, where the South Tibetan lithosphere is thought to be exposed to a higher heat flux and more abundant Cenozoic magmatism (e.g. Chung et al., 2005; Kapp et al., 2005; Ding et al., 2007), and is therefore possibly weaker.

In the analogue experiment, the piston produces a constant kinematic boundary condition which in principle does not resemble any dynamic natural condition. At the scale of the collision zone, this setting mimics the far field forces that sustain the northward motion of India. Here, the enigmatic label far field simply refers to the forces that contribute to plate tectonics but that originate remotely from plate boundaries. They are not many in the plate dynamics budget (e.g., Forsyth and Uyeda, 1975), and essentially refer to mantle drag from the underlying mantle convection. Active mantle drag is essential to drive plates against or away from each other, and provides a dynamic explanation to the observed kinematics of plate boundaries (Husson, 2012). It may contribute to propel subducting plates (Alvarez, 2010), as it is the case for India–Eurasia (e.g. Becker and Faccenna, 2011), but is equally efficient in pushing the upper plate towards a convergent zone, as it is for example the case for the South America–Nazca convergent system (Husson et al., 2012b). Alternative models to active mantle drag also explain the fast convergence of India with the support from forces arising from the South, by the inception of the slab into the lower mantle that would excite a larger convection cell (Faccenna et al., 2013), by reinforced push from the Reunion plume (van Hinsbergen et al., 2005), or by a weaker, lubricating as-

thenosphere that restrain the resistance to the northward motion of India (Cande and Stegman, 2011).

The force balance at the plate boundary constantly evolve and should modulate plate convergence at all times (e.g. Iaffaldano et al., 2011; Clark, 2012), but regardless the northward motion of India continued at a rate in excess of 50 mm/yr since the beginning of the collision (e.g. Patriat and Achache, 1984; Molnar and Stock, 2009; van Hinsbergen et al., 2005, which supports the hypothesis of a primordial role for far-field forces. The explanation is to be found at a larger scale. The Indian collision is embedded in a much wider convergent system, namely the Tethyan subduction zone, from the Mediterranean to the Banda arc, driving the dynamics of the global system and constraining the force balance at the boundary between India and Eurasia. This makes the assumption of constant convergence rate during the collision an acceptable simplification. Indeed, our model adequately reproduces the horizontal motion of the indenter, analogue of the motion of India.

6. Conclusion

We explore the subduction dynamics of the continental lithosphere, a process which is increasingly documented below Tibet. Of course, the positive buoyancy of such a slab is ruled out as the driving force because it refrains subduction. In previously published experiments, it has been proposed that the horizontal push of the piston, whose force is transmitted first to the indenter, and second to the upper plate, was the main driving force that have been called the tectonic force (Replumaz et al., 2016). At the lithospheric scale, the horizontal tectonic force is higher than the bending of the backwall plate and the lithosphere/lithosphere interface resistances, allowing for its bending. In this paper we show that at the mantle scale, as soon as the indenter bends and enters the mantle, it changes the mantle circulation in particular below the upper plate. The initiation of the continental subduction reverses the motion of the trench, and as the trench advances the upper plate starts to thick. With a viscosity lower for the upper than for the backwall plate, such differential thicking generates a smaller convective cell below the upper plate, favoring the initiation of the backwall plate with the thicker upper plate acting as a buttress. Then during the rest of the experiment, we observe a continuous trench advance, generating a continuous enhance of the indenter slab curvature and a dominant horizontal motion of the mantle. This forward horizontal flow in front of the advancing indenter first passively transported (advection) the backwall slab in the mantle. When the length of the slab increases, the flow is slightly perturbed by the slab and a dynamic mantle push occurred on the backwall slab.

Appendix A. Supplementary material

Supplementary material related to this article can be found online at https://doi.org/10.1016/j.epsl.2018.08.050.

References

Alvarez, W., 2010. Protracted continental collisions argue for continental plates driven by basal traction. Earth Planet. Sci. Lett. 296, 434–442.

Bajolet, F., Replumaz, A., Lainé, R., 2013. Orocline and syntaxes formation during subduction and collision. Tectonics 32, 1529–1546. https://doi.org/10.1002/tect.20087.

Becker, T.W., Faccenna, C., 2011. Mantle conveyor beneath the Tethyan collisional belt. Earth Planet. Sci. Lett. 310, 453–461. https://doi.org/10.1016/j.epsl.2011.08.021.

Bellahsen, N., Faccenna, C., Funiciello, F., 2005. Dynamics of subduction and plate motion in laboratory experiments: Insights into the "plate tectonics" behavior of the Earth. J. Geophys. Res. 110, B01401. https://doi.org/10.1029/2004JB002999.

Burtman, V.S., Molnar, P., 1993. Geological and geophysical evidence for deep subduction of continental crust beneath the Pamir. Spec. Pap., Geol. Soc. Am. 281, 76.

Cande, S.C., Stegman, D.R., 2011. Indian and African plate motions driven by the push force of the Reunion plume head. Nature 475, 47–52. https://doi.org/10.1038/nature10174.

Capitanio, F.A., Morra, G., Goes, S., Weinberg, R.F., Moresi, L., 2010. India–Asia convergence driven by the subduction of the Greater Indian continent. Nat. Geosci. 3, 136–139. https://doi.org/10.1038/NGEO725.

Capitanio, F.A., Replumaz, A., Riel, N., 2015. Reconciling subduction dynamics during Tethys closure with large-scale Asian tectonics: insights from numerical modeling. Geochem. Geophys. Geosyst. 16, 962–982. https://doi.org/10.1002/2014GC005660.

Chatelain, J.L., Roecker, S.W., Hatzfeld, D., Molnar, P., 1980. Microearthquake seismicity and fault plane solutions in the HinduKush region and their tectonic implications. J. Geophys. Res. 85, 1365–1387.

Chung, S.-L., et al., 2005. Tibetan tectonic evolution inferred from spatial and temporal variations in post-collisional magmatism. Earth-Sci. Rev. 68, 173–196.

Clark, M.K., 2012. Continental collision slowing due to viscous mantle lithosphere rather than topography. Nature 483. https://doi.org/10.1038/nature10848.

DeCelles, P.G., Robinson, D.M., Zandt, G., 2002. Implications of shortening in the Himalayan fold-thrust belt for uplift of the Tibetan Plateau. Tectonics 21, 1062. https://doi.org/10.1029/2001TC001322.

Ding, L., Kapp, P., Yue, Y., Lai, Q., 2007. Postcollisional calc–alkaline lavas and xenoliths from the southern Qiangtang terrane, central Tibet. Earth Planet. Sci. Lett. 254, 28–38.

Faccenna, C., Becker, T.W., Conrad, C.P., Husson, L., 2013. Mountain building and mantle dynamics. Tectonics 32, 80–93. https://doi.org/10.1029/2012TC003176.

Forsyth, D., Uyeda, S., 1975. On the relative importance of the driving forces of plate motion. Geophys. J. R. Astron. Soc. 43, 163–200.

Funiciello, F., Faccenna, C., Giardini, D., Regenauer-Lieb, K., 2003. Dynamics of retreating slabs, 2. Insights from three-dimensional laboratory experiments. J. Geophys. Res. 108 (B4), 2207. https://doi.org/10.1029/2001jb000896.

Funiciello, F., Faccenna, C., Giardini, D., 2004. Role of lateral mantle flow in the evolution of subduction system: insights from 3-D laboratory experiments. Geophys. J. Int. 157, 1393–1406.

Funiciello, F., Moroni, M., Piromallo, C., Faccenna, C., Cenedese, A., Bui, H.A., 2006. Mapping the flow during retreating subduction: laboratory models analyzed by feature tracking. J. Geophys. Res. 111, B03402. 03410.01029/02005JB003792.

Goussin, F., Cordier, C., Guillot, S., Boulvais, P., Roperch, P., Replumaz, A., Schulmann, K., Dupont-Nivet, G., Guo, Z., submitted for publication. Metasomatized mantle and growth of the Tibet Plateau. Earth Planet. Sci. Lett.

Hetenyi, G., Cattin, R., Brunet, F., Bollinger, L., Vergne, J., Nabelek, J., Diament, M., 2007. Density distribution of the India plate beneath the Tibetan Plateau: geophysical and petrological constraints on the kinetics of lower-crustal eclogitization. Earth Planet. Sci. Lett. 264. https://doi.org/10.1016/j.epsl.2007.09.036.

Holmes, A., 1929. Radioactivity and earth movements. Trans. Geol. Soc. Glasg. 18, 559–606.

Husson, L., 2012. Trench migration and upper plate strain over a convecting mantle. Phys. Earth Planet. Inter. 212, 32–43. https://doi.org/10.1016/j.pepi.2012.09.006.

Husson, L., Guillaume, B., Funiciello, F., Faccenna, C., Royden, L.H., 2012a. Unravelling topography around subduction zones from laboratory models. Tectonophysics 526, 5–15. https://doi.org/10.1016/j.tecto.2011.09.001.

Husson, L., Conrad, C.P., Faccenna, C., 2012b. Plate motions, Andean orogeny, and volcanism above the South Atlantic convection cell. Earth Planet. Sci. Lett. 317, 126–135. https://doi.org/10.1016/j.epsl.2011.11.040.

Iaffaldano, G., Husson, L., Bunge, H.-P., 2011. Monsoon speeds up Indian plate motion. Earth Planet. Sci. Lett. 304, 503–510. https://doi.org/10.1016/j.epsl.2011.02.026.

Kapp, P., Yin, A., Harrison, T.M., Ding, L., 2005. Cretaceous–Tertiary shortening, basin development, and volcanism in central Tibet. Geol. Soc. Am. Bull. 117, 865–878.

Kind, R., et al., 2002. Seismic images of crust and upper mantle beneath Tibet: evidence for Eurasian plate subduction. Science 298, 1219–1221. https://doi.org/10.1126/science.1078115.

Kufner, S.-K., et al., 2016. Deep India meets deep Asia: lithospheric indentation, delamination and break-off under Pamir and Hindu Kush (Central Asia). Earth Planet. Sci. Lett. 435, 171–184. https://doi.org/10.1016/j.epsl.2015.11.046.

Luth, S., Willingshofer, E., Sokoutis, D., Cloetingh, S., 2010. Analogue modelling of continental collision: influence of plate coupling on mantle lithosphere subduction, crustal deformation and surface topography. Tectonophysics 484, 87–102. https://doi.org/10.1016/j.tecto.2009.08.043.

Liao, J., Gerya, T., Thielmann, M., Webb, A.G., Kufner, S.-K., Yin, A., 2017. 3D geodynamic models of continental subduction with opposite polarities in the Hindu Kush–Pamir orogenic system, northwestern Tibetan Plateau. Earth Planet. Sci. Lett. 480, 133–146. https://doi.org/10.1016/j.epsl.2017.10.005.

Mattauer, M., 1986. Intracontinental subductions in Tertiary mountains belts of Asia – relationships with strike-slip faults. Bull. Soc. Géol. Fr. 2, 143–157.

Mechie, J., Yuan, X., Schurr, B., Schneider, F., Sippl, C., Ratschbacher, L., Minaev, V., Gadoev, M., Oimahmadov, I., Abdybachaev, U., Moldobekov, B., Orunbaev, S., Negmatullaev, S., 2012. Crustal and uppermost mantle velocity structure along a profile across the Pamir and southern Tien Shan as derived from project TIPAGE wide-angle seismic data. Geophys. J. Int. 188, 385–407. https://doi.org/10.1111/j.1365-246X.2011.05278.x.

Molnar, P., Stock, J.M., 2009. Slowing of India's convergence with Eurasia since 20 Ma and its implications for Tibetan mantle dynamics. Tectonics 28, TC3001. https://doi.org/10.1029/2008TC002271.

Nábělek, J., Hetényi, G., Vergne, J., Sapkota, S., Kafle, B., Jiang, Mei, Su, Heping, Chen, John, Huang, Bor-Shouh, The Hi-CLIMB Team, 2009. Underplating in the Himalaya–Tibet Collision Zone revealed by the Hi-CLIMB experiment. Science 325. https://doi.org/10.1126/science.1167719.

Negredo, A.M., Replumaz, A., Villasenor, A., Guillot, S., 2007. Modeling the evolution of continental subduction processes in the Pamir–Hindu Kush region. Earth Planet. Sci. Lett. 259, 212–225. https://doi.org/10.1016/j.epsl.2007.04.043.

Patriat, Ph., Achache, J., 1984. India–Eurasia collision chronology has implications for crustal shortening and driving mechanisms of plates. Nature 311, 615–621.

Piromallo, C., Becker, T.W., Funiciello, F., Faccenna, C., 2005. Three-dimensional instantaneous mantle flow induced by subduction. Geophys. Res. Lett. 33. https://doi.org/10.1029/2005GL025390.

Replumaz, A., Guillot, S., Villaseñor, A., Negredo, A.M., 2013. Amount of Asian lithospheric mantle subducted during the India/Asia collision. Gondwana Res. 24, 936–945. https://doi.org/10.1016/j.gr.2012.07.019.

Replumaz, A., Funiciello, F., Reitano, R., Faccenna, C., Balon, M., 2016. Double subduction of continental lithosphere, a key to form wide plateau. Geology. https://doi.org/10.1130/G38276.1.

Schneider, F.M., Yuan, X., Schurr, B., Mechie, J., Sippl, C., Haberland, C., Minaev, V., Oimahmadov, I., Gadoev, M., Radjabov, N., Abdybachaev, U., Orunbaev, S., Negmatullaev, S., 2013. Seismic imaging of subducting continental lower crust beneath the Pamir. Earth Planet. Sci. Lett. 375, 101–112. https://doi.org/10.1016/j.epsl.2013.05.015.

Spurlin, M.S., Yin, A., Horton, B.K., Zhou, J., Wang, J., 2005. Structural evolution of the Yushu–Nangqian region and its relationship to syncollisional igneous activity, east-central Tibet. Geol. Soc. Am. Bull. 117, 1293–1317. https://doi.org/10.1130/B25572.1.

Tapponnier, P., Xu, Z.Q., Roger, F., Meyer, B., Arnaud, N., Wittlinger, G., Yang, J.S., 2001. Oblique stepwise rise and growth of the Tibet plateau. Science 294, 1671–1677.

Thielicke, W., Stamhuis, E.J., 2014. PIVlab – towards user-friendly, affordable and accurate digital particle image velocimetry in Matlab. J. Open Res. Softw. 2 (1), e30. https://doi.org/10.5334/jors.bl.

Turcotte, D.L., Schubert, G., 1982. Geodynamics Application of Continuum Physics to Geological Problems. John Wiley, New York.

van Hinsbergen, D.J.J., Steinberger, B., Doubrovine, P.V., Gassmoeller, R., 2005. Acceleration and deceleration of India–Asia convergence since the Cretaceous: roles of mantle plumes and continental collision. J. Geophys. Res. 116, B06101. https://doi.org/10.1029/2010jb008051.

Weijermars, R., 1986. Flow behavior and physical-chemistry of bouncing putties and related polymers in view of tectonic laboratory applications. Tectonophysics 124 (3–4), 325–358. https://doi.org/10.1016/0040-1951(86)90208-8.

Weijermars, R., Schmeling, H., 1986. Scaling of Newtonian and non Newtonian fluid dynamics without inertia for quantitative modelling of rock flow due to gravity (including the concept of rheological similarity). Phys. Earth Planet. Inter. 43, 316–330.

Willingshofer, E., Sokoutis, D., Luth, S.W., Beekman, F., Cloetingh, S., 2013. Subduction and deformation of the continental lithosphere in response to plate and crust–mantle coupling. Geology 41 (12), 1239–1242. https://doi.org/10.1130/G34815.1.